Design of Hybrid Optical Amplifiers for High Capacity Optical Transmission

Seung Kwan Kim, Sun Hyok Chang, Jin Soo Han, and Moo Jung Chu

This paper describes our design of a hybrid amplifier composed of a distributed Raman amplifier and erbium-doped fiber amplifiers for C- and L-bands. We characterize the distributed Raman amplifier by numerical simulation based on the experimentally measured Raman gain coefficient of an ordinary single mode fiber transmission line. In single channel amplification, the crosstalk caused by double Rayleigh scattering was independent of signal input power and simply given as a function of the Raman gain. The double Rayleigh scattering induced power penalty was less than 0.1 dB after 1000 km if the on-off Raman gain was below 21 dB. For multiple channel amplification, using commercially available pump laser diodes and fiber components, we determined and optimized the conditions of three-wavelength Raman pumping for an amplification bandwidth of 32 nm for C-band and 34 nm for L-band. After analyzing the conventional erbium-doped fiber amplifier analysis in C-band, we estimated the performance of the hybrid amplifier for long haul optical transmission. Compared with erbium-doped fiber amplifiers, the optical signal-to-noise ratio was calculated to be higher by more than 3 dB in the optical link using the designed hybrid amplifier.

Manuscript received Sept. 21, 2001; revised Feb. 18, 2002.

Seung Kwan Kim (phone: +82 42 860 6143, e-mail: skim@etri.re.kr), Sun Hyok Chang (e-mail: shchang@etri.re.kr), Jin Soo Han (e-mail: hanjinsoo@etri.re.kr), and Moo Jung Chu (e-mail: mjc@etri.re.kr) are with Electronics and Telecommunications Research Institute, Daejeon, Korea.

I. INTRODUCTION

As the demand for higher transmission capacity in wavelength division multiplexing (WDM) systems increases, channel speed, channel number, and spectral efficiency need to be upgraded. To this end, Raman amplifiers have become essential in overcoming the limitations of the bandwidth, noise figure (NF), and output power of conventional doped fiber amplifiers [1]-[8]. Recently, great attention has been paid to the Raman amplifiers used in conjunction with erbium-doped fiber amplifiers (EDFAs) to form hybrid amplifiers, especially when the system capacity needs to be upgraded by raising channel speed and spectral efficiency without bandwidth expansion [3]-[8].

In the hybrid amplifiers, the NF can be effectively reduced without changing the output power [1]. Both discrete Raman [3], [4] and distributed Raman amplifiers (DRAs) [5]-[8] have been used for hybrid amplifiers. For long haul transmission, a DRA is more desirable since the transmission line itself can be used as a gain medium simply by adding a Raman pump module (RPM), and a previously installed EDFA can also be used by making a slight modification according to the changed input power and spectrum.

In designing hybrid DRA/EDFAs, it is important to optimize the Raman gain in terms of the amplifier noise because the increment of Raman gain increases double Rayleigh scattering (DRS) noise as well as amplified spontaneous emission (ASE) noise. In addition, the NF of the following EDFA also increases because of the increased input power. Therefore, it is essential to understand the behavior of hybrid DRA/EDFAs, which are dependent on pump power, the corresponding Raman gain, and the corresponding EDFA input.

This paper analyzes the characteristics of DRAs by numerical simulation based on the experimentally measured Raman

gain coefficient using an ordinary single mode fiber (SMF). We evaluate the validity of the numerical simulation by comparing it with the experimental measurement using a nonzero dispersion shifted fiber (NZ-DSF). In single channel amplification, we examine the ASE and DRS noise behavior as the Raman gain increases and then estimate the Raman gain limitation due to the DRS noise induced penalty. In multiple channel amplification, we determine the optimum pump wavelengths for a bandwidth of 66 nm (32 nm for C-band and 34 nm for L-band) and calculate the maximum Raman gain that is readily available with the current active and passive component technology. We then determine by numerical simulation the optimum EDF lengths for a C-band EDFA to produce the minimum noise figure. Finally, we estimate the performance of the resultant hybrid amplifier in C-band to show the applicability of the amplifier to long haul optical transmission.

II. CONFIGURATION OF THE HYBRID AMPLIFIER

A hybrid amplifier consists of a DRA and EDFAs as shown in Fig. 1. A DRA is composed of a Raman pump module (RPM) and a power clamping module (PCM) that keeps the input power to the EDFA constant with a voltage controlled attenuator (VCA) and a signal tapping coupler with a negative feedback method. The DRA is pumped by several pump wavelengths in a backward direction to achieve a wide gain bandwidth covering both C-band (1530–1562 nm) and L-band (1571–1605 nm) with minimized pump induced signal fluctuation [9]. Three or more pump wavelengths are multiplexed by a pump WDM combiner (PWC) that is commercially available. Each pump wavelength is provided by two pump laser diodes (LDs) with the same wavelength multiplexed by a polarization beam combiner (PBC). Each pump LD is wavelength stabilized using an external fiber Bragg grating (FBG). The multiplexed pump beams are then launched into a transmission fiber using a pump/signal WDM coupler (PSWC). The Raman amplified WDM signals are power regulated by the PCM and passed to the C- and L-band EDFAs after C/L-band splitting. Each EDFA has two amplification gain blocks (GBs) separated by an inter-stage functional block for gain flattening and dispersion compensation. Each GB consists of EDF, a forward (Fwd) and backward (Bwd) PSWC with optical isolators (OIs), 980 nm or 1480 nm pump LDs, and tap couplers for input and output monitoring. The amplified WDM signals from the C- and L-band EDFAs are then combined with a C/L-band combiner and conveyed to the next transmission fiber.

III. THEORETICAL MODEL OF THE DRA

The evolution of Raman pumps and WDM signals passing through the transmission fiber is governed by (1) – (3) [10], [11].

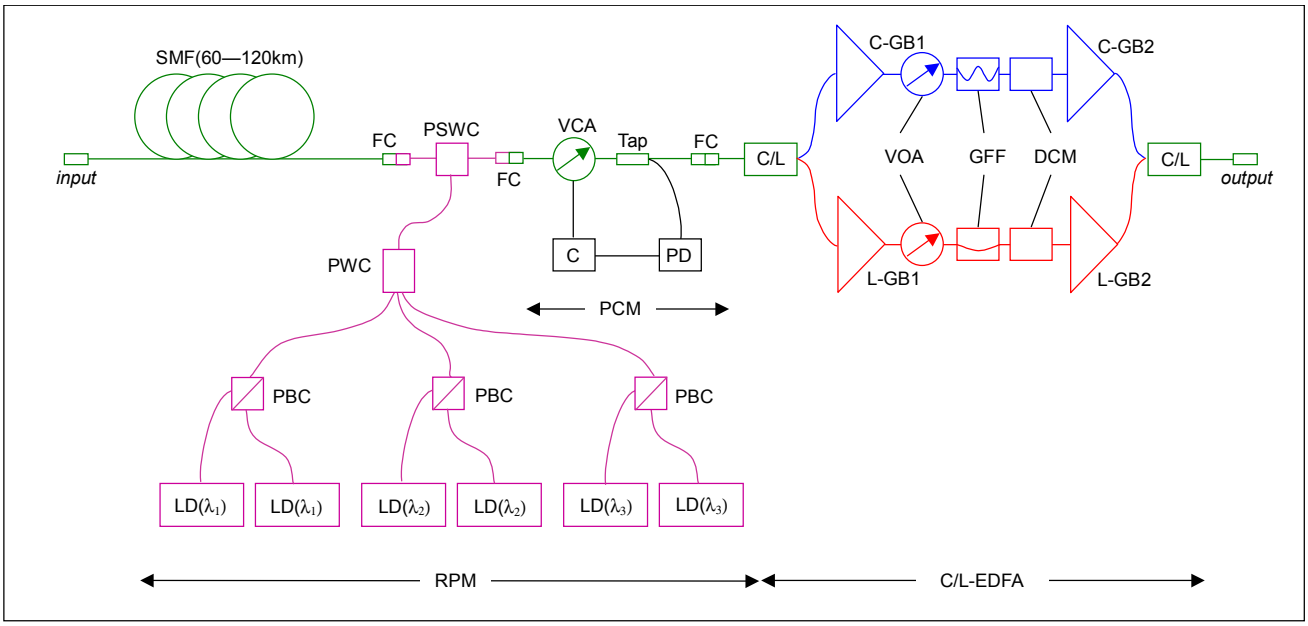

Fig. 1. Configuration of the hybrid optical amplifier. C, controller (proportional-integral contol); C-GB, C-band gain block; L-GB, L-band gain block; C/L, C/L-band WDM coupler; DCM, dispersion compensating module; FC, fiber connector; GFF, gain flattening filter; LD, pump laser diodes; PBC, polarization beam combiner; PWC, pump WDM combiner; PSWC, pump/signal WDM coupler; PD, photo-diode; PCM, power clamping module; RPM, Raman pump module; Tap, tap coupler; VCA, voltage controlled attenuator; VOA, variable optical attenuator.

$$P_i^{\pm} = S_i^{\pm} + N_i^{\pm} \tag{1}$$

$$\begin{aligned}\frac{dS_i^{\pm}}{dz} = &\mp\alpha_i S_i^{\pm} \pm \sum_{\nu_j>\nu_i} C_{pol}\frac{g_R(\lambda_j,\nu_j-\nu_i)}{A_{ij}}\left[P_j^{+}+P_j^{-}\right]S_i^{\pm} \\ &\mp \sum_{\nu_j<\nu_i} C_{pol}\frac{\nu_i g_R(\lambda_i,\nu_i-\nu_j)}{\nu_j A_{ij}}\left[P_j^{+}+P_j^{-}\right]S_i^{\pm} \\ &\mp \sum_{\nu_j<\nu_i} \frac{\nu_i g_R(\lambda_i,\nu_i-\nu_j)}{\nu_j A_{ij}} 2h\nu_j\Delta\nu\left(1+\frac{1}{e^{\frac{h(\nu_i-\nu_j)}{\mathrm{kT}}}-1}\right)S_i^{\pm}\end{aligned} \tag{2}$$

$$\begin{aligned}\frac{dN_i^{\pm}}{dz} = &\mp\alpha_i N_i^{\pm} \pm \gamma_i P_i^{\mp} \pm \sum_{\nu_j>\nu_i} C_{pol}\frac{g_R(\lambda_j,\nu_j-\nu_i)}{A_{ij}}\left[P_j^{+}+P_j^{-}\right]N_i^{\pm} \\ &\pm \sum_{\nu_j>\nu_i} \frac{g_R(\lambda_j,\nu_j-\nu_i)}{A_{ij}}\left[P_j^{+}+P_j^{-}\right]h\nu_i\Delta\nu\left(1+\frac{1}{e^{\frac{h(\nu_j-\nu_i)}{\mathrm{kT}}}-1}\right) \\ &\mp \sum_{\nu_j<\nu_i} C_{pol}\frac{\nu_i g_R(\lambda_i,\nu_i-\nu_j)}{\nu_j A_{ij}}\left[P_j^{+}+P_j^{-}\right]N_i^{\pm} \\ &\mp \sum_{\nu_j<\nu_i} \frac{\nu_i g_R(\lambda_i,\nu_i-\nu_j)}{\nu_j A_{ij}} 2h\nu_j\Delta\nu\left(1+\frac{1}{e^{\frac{h(\nu_i-\nu_j)}{\mathrm{kT}}}-1}\right)N_i^{\pm}\end{aligned} \tag{3}$$

To treat the Rayleigh back scattering as a noise source, we separated the pure signal part, S_i, and the noise part, N_i, out of the optical power of the i-th wavelength component. In (1) – (3), C_{pol} is the polarization scrambling factor between the two optical beams that is assumed to be 0.5 because each pump beam has two orthogonal polarizations and the signal polarizations are randomly allocated in front of the transmission fiber. α_i and γ_i are the attenuation coefficient and Rayleigh backscattering coefficient of the i-th wavelength, respectively. A_{ij} is the effective interaction area defined in [12], which is equal to the average value of the effective mode area of the two wavelengths if the Gaussian approximation of the fiber mode is used as shown in (4) – (6).

$$I(r) = I_0\psi(r) = I_0\exp\left[-\left(\frac{r}{\omega}\right)^2\right] \tag{4}$$

$$A_{eff} = 2\pi\omega^2 \tag{5}$$

$$A_{ij} = \frac{\oint_A \psi_i(r)da \times \oint_A \psi_j(r)da}{\oint_A \psi_i(r)\psi_j(r)da} = \pi\omega_i^{\,2} + \pi\omega_j^{\,2} = \frac{A_{eff,i} + A_{eff,j}}{2} \tag{6}$$

The Raman gain coefficient (RGC), $g_R(\lambda_1, \nu_i - \nu_j)$, is given as a function of the frequency difference between the two wavelengths as well as a wavelength of light acting as a pump, because the peak Raman gain coefficient is scaled inversely proportional to the pump wavelength [10]. The constant k and h are Boltzmann's constant and Planck's constant, respectively.

The second term in the right hand side of (2) represents the gain by optical signals with shorter wavelengths, while the third and the fourth terms represent absorption by optical signals with longer wavelengths and the ASE generated by the signal at the i-th wavelength, respectively. The second term in the right hand side of (3) represents Rayleigh backscattering, which is treated as a noise source, and the fourth term represents the addition of the ASE noise generated between the optical frequencies ν_i and $\nu_i + \Delta\nu$ by optical signals with shorter wavelengths. The other terms in (3) have the same meaning as those in (2).

In order to theoretically analyze the DRA, the RGC needs to be measured for a given optical fiber; to do this, we used four single mode fiber (SMF) spools, each with a length of about 20 km. The fiber was a matched-cladding type SMF with an average mode field diameter of 9.37 μm at 1310 nm and a cut-off wavelength of 1270 nm. The RGC can be obtained by measuring the small signal Raman gain (G) on a log scale with a given pump power (P_p), an effective interaction area (A_{eff}) between the pump and signal, an attenuation coefficient of the pump (α_p), and the fiber length (L) using (7) and (8) [10].

$$g_R(\lambda_p, \nu_p - \nu_s) = g_{R,\max}(\lambda_p)\Gamma(\nu_p - \nu_s) = \frac{GA_{eff}}{4.34C_{pol}P_pL_{eff}} \tag{7}$$

$$L_{eff} = \frac{1-\exp(-\alpha_p L)}{\alpha_p}, \tag{8}$$

where $g_{R,max}(\lambda_p)$ is the peak of the RGC with a pump wavelength of (λ_p) and $\Gamma(\nu_p - \nu_s)$ is the normalized RGC by $g_{R,max}(\lambda_p)$.

For a signal source we used a tunable laser diode with a wavelength tuned by 1.0 nm from 1520.0 nm to 1620.0 nm and an input power of –20 dBm. The pump wavelengths were 1445.7 nm and 1485.1 nm. With these wavelengths it was possible to measure the Raman gain in a range from 4.6 THz to 22.3 THz. To measure the Raman gain between 0 and 4.6 THz, a new pump source was constructed at a wavelength of 1530.0 nm. This new pump source was a tunable laser diode amplified by high power EDFA with a bandpass filter to reject unwanted ASE noise [13]. Strictly speaking, A_{eff} in (7) has a different value for a different pump and signal wavelength combination.

However, it differs by only 0.28 dB for signal wavelengths from 1520.0 nm to 1620.0 nm, which is less than the level flatness of the optical spectrum analyzer (OSA) of ±0.2 dB. Therefore, the same A_{eff} estimated at the Raman peak wavelength was used for each pump wavelength. For 1445.7 nm and 1485.1 nm, the effective interaction areas were 84.8 μm^2 and 89.1 μm^2, respectively. For the 1530.0 nm pump, the Raman gain peak was located outside of the measurement range, and the measurement data was used only to connect the gap of the line shape function $\Gamma(v_p - v_s)$, between 0 and 4.6 THz. To minimize errors in the measurement, the Raman gain was measured for 20, 40, 60, and 80 km, and the RGC was averaged over the fiber length. For the 1445.7 nm and 1485.1 nm pump, the gain peak wavelengths were 1545.0 nm and 1590.0 nm resulting in a Raman frequency shift of 13.3 THz. The average peak values of the measured RGC divided by A_{eff} were 0.88×10^{-3} m^{-1}W^{-1} for the 1445.7 nm pump and 0.80×10^{-3} m^{-1}W^{-1} for the 1485.1 nm pump. Since the RGC is scaled inversely proportional to the pump wavelength, the scalar product of the RGC and the pump wavelength is an important parameter for simulation using arbitrary multiple pump wavelengths. From the two average peak values, the estimated average value of $g_{R,max}(\lambda_p)\times\lambda_p$ for the two pump wavelengths was 1.07×10^{-19} m^2/W with less than 1.2 % error. This was much less than the overall measurement error caused by the level flatness of the OSA and the polarization dependent loss (PDL) of the fiber components. Figure 2 shows the measured Raman gain coefficient from 0 to 22.3 THz normalized by its maximum value.

For the computer simulation, the measured attenuation coefficients of the pump and signal wavelengths were used and the Rayleigh backscattering coefficient was taken from Ref. [14],

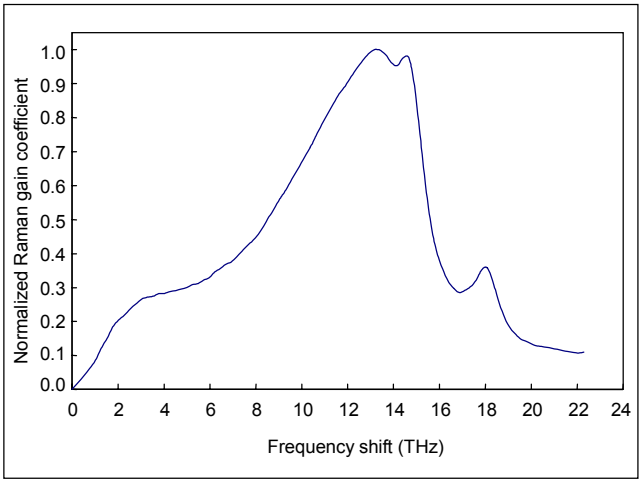

Fig. 2. Measured Raman gain coefficient normalized by the maximum value.

assuming that it was not significantly different. In solving (1) – (3), the Runge-Kutta method with a 4th order was applied with a relaxation method to find correct solutions for all signals. The length was divided by 50 and it was proved that the error was less than 0.01 dB compared with a length division of 100. It took less than 3 min. to calculate 3 pumps and 160 channels using a Pentium III 933 MHz microprocessor.

IV. EVALUATION OF THE NUMERICAL SIMULATION

Before moving into the characterization and design of the DRA, we examined the validity of the numerical simulation using nonzero dispersion shifted fiber (NZ-DSF), where the RGC divided by A_{eff} was 1.5×10^{-3} and 1.3×10^{-3} m^{-1}W^{-1} for the 1445.7 and 1485.1 nm pumps, respectively. The average cutoff wavelength and mode field diameter of the NZ-DSF was 1069 nm and 8.25 μm, respectively. The calculated effective interaction areas were 49.2 and 52.7 μm^2 for pump-signal combinations of 1445.7 nm to 1545.0 nm and 1485.1 nm to 1590.0 nm, respectively. The estimated average value of $g_{R,max}\times\lambda_p$ was the same as that of the SMF, that is, 1.1×10^{-19} m^2/W with less than 2% error for the two pump-signal combinations. As with the SMF, the normalized RGC profile for the NZ-DSF was also obtained with the two pump wavelengths and the 1530.0 nm pump source.

When the single channel input of –20 dBm tuned from 1520 to 1620 nm was launched into NZ-DSF with a length of 80 km, the on-off Raman gain and the equivalent NF were measured and are shown as symbols in Fig. 3, where the pump power at 1485.1 nm was varied from 80 mW to 110 mW while it was fixed at 135 mW at 1445.7 nm. The numerical simulation results shown as solid lines agreed well with the experimental data. The maximum difference between the experiment and numerical simulation was less than 0.3 dB for the gain and 0.5 dB for the NF; these are comparable to the error bounds that are due to PDL, the wavelength uniformity of the PSWC, and the level flatness of the OSA.

For the measurement of multiple channel amplification, 24 continuous-wave channels in C-band and 22 in L-band with two intensity modulated link control channels were launched into the 80 km NZ-DSF as shown in Fig. 4. The total input powers were 18.7 dBm for C-band and 19.3 dBm for L-band. The off-level in Fig. 5 corresponded to the estimated output power when the SRS effect was ignored; it was calculated using the measured fiber attenuation coefficient. Without pumping, the channels became tilted because of the SRS effect. When the pump power at 1485.1 nm was varied from 20 mW to 100 mW with a fixed pump power of 135 mW at 1445.7 nm,

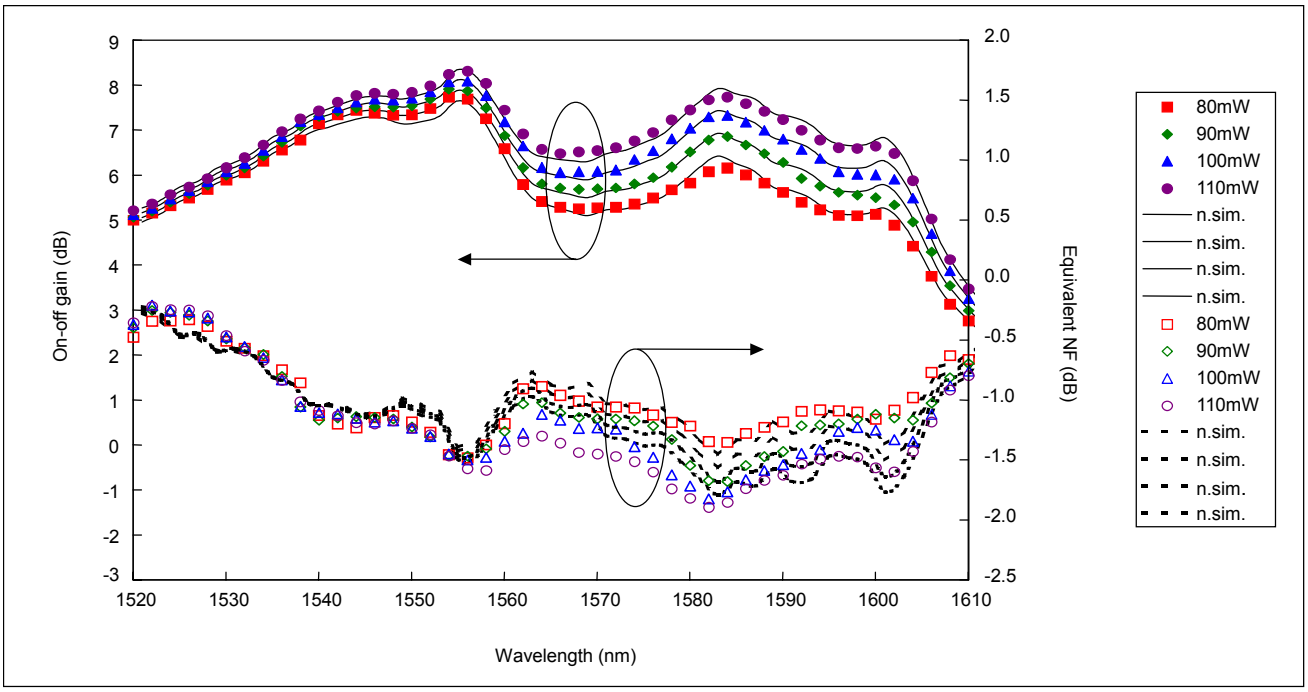

Fig. 3. Small signal on-off Raman gain and NF spectrum of DRA using NZDSF 80 km for various Raman pump powers. The numbers in the legend box correspond to pump power at 1485.1 nm, while the pump power at 1445.7 nm was fixed at 135 mW. n.sim., numerical simulation.

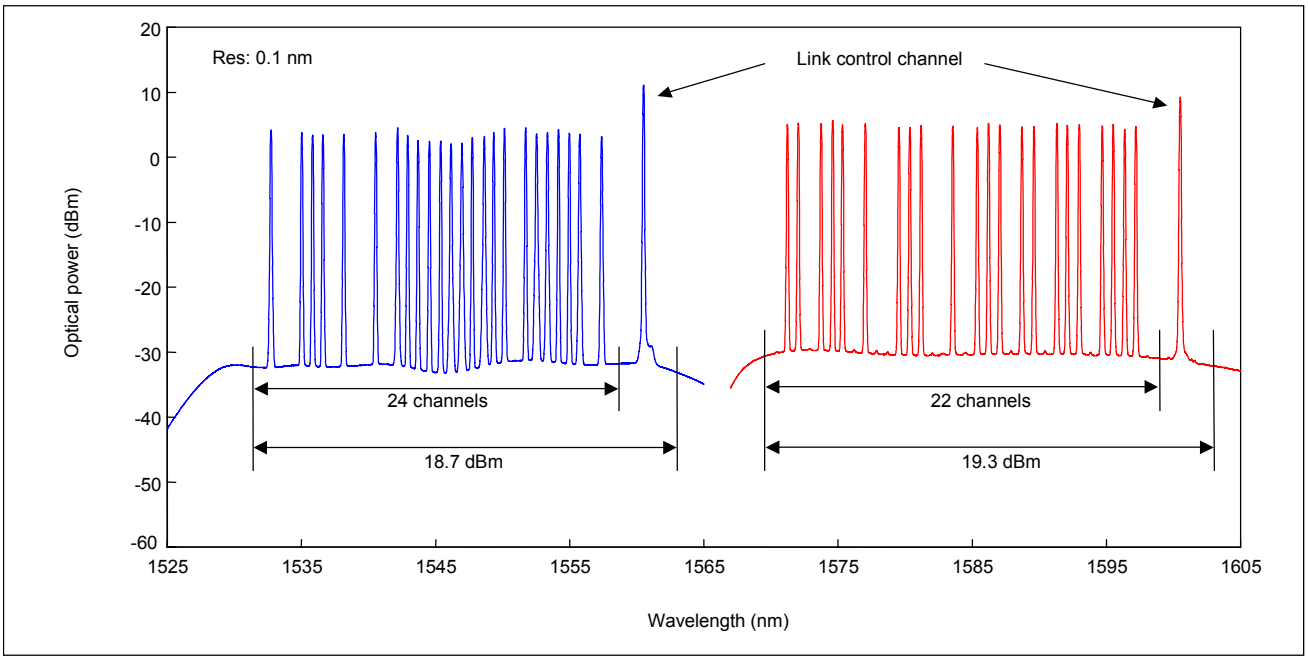

Fig. 4. Input spectrum for multiple channel amplification measurement of DRA using NZDSF.

the output power profiles changed as shown in Fig. 5. Again, the experimental data agreed reasonably well with the numerical simulation. However, the measured NF data could not be compared with the numerical simulation because they exhibited enormous errors owing to the high input ASE level.

V. SINGLE CHANNEL AMPLIFICATION

For the single channel amplification, 1450 nm and 1550 nmwere chosen as the pump and signal wavelengths, respectively. The bandwidth was set at 0.1 nm. The fiber length was

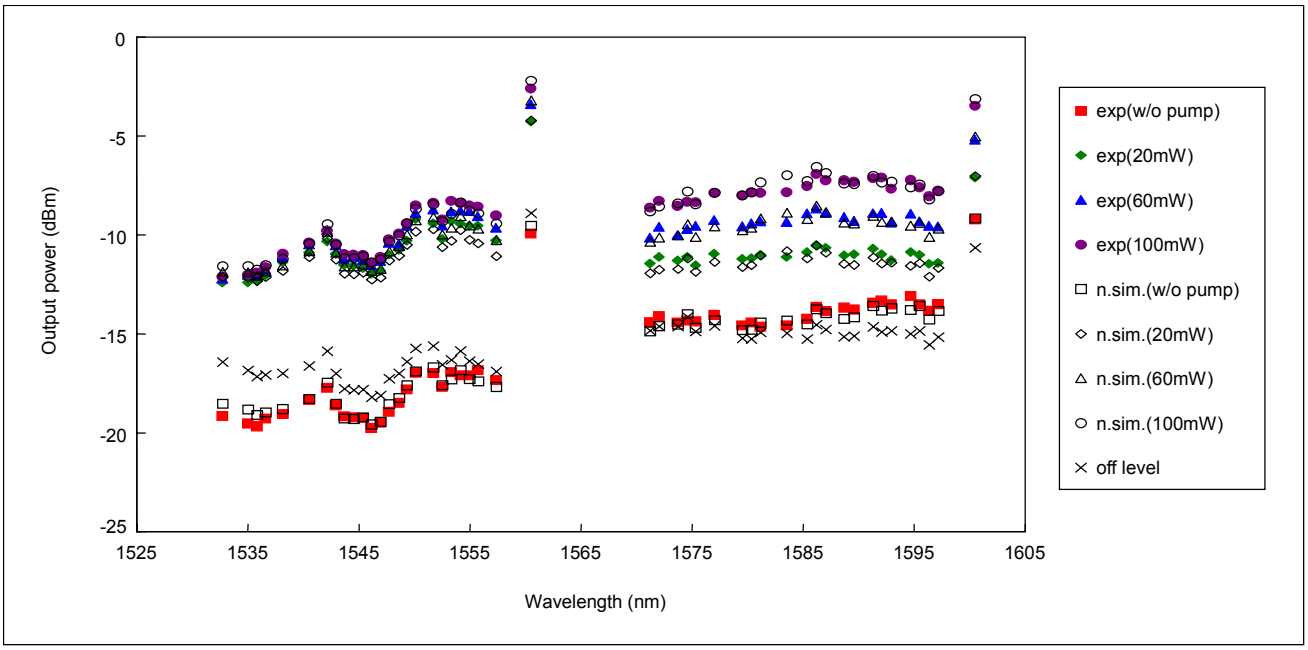

Fig. 5. Output spectrum of DRA using NZDSF 80 km for various pump powers. The numbers in the legend box correspond to pump power at 1485.1 nm, while the pump power at 1445.7 nm was fixed at 165 mW. exp, experiment; n.sim., numerical simulation.

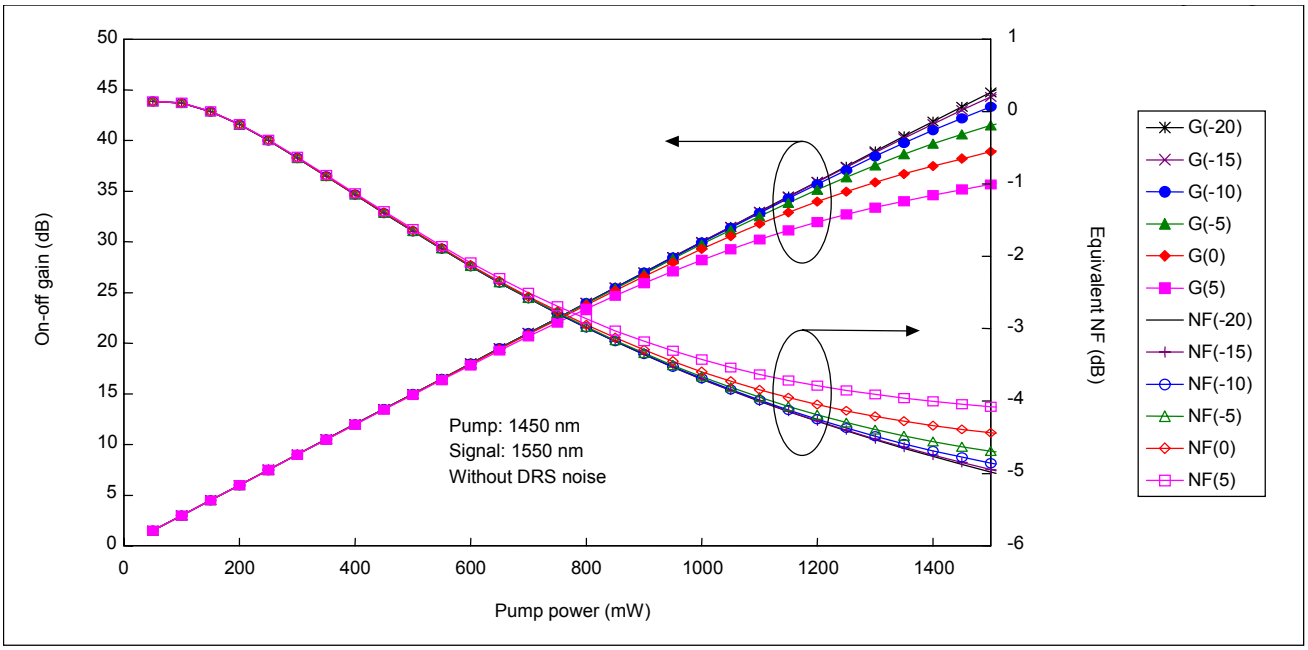

Fig. 6. On-off Raman gain and equivalent NF versus pump power for various input power levels without DRS. The numbers in the legend box correspond to input power levels in dBm.

assumed to be 80 km. Because the increasing rate of gain was less than that of the ASE at the beginning of the pump power, the OSNR decreased as the pump power increased (Fig. 7) until the on-off Raman gain became about 9 dB when the pump power was about 300 mW (Fig. 6). After that, the OSNR increased monotonically. If DRS was ignored, the noise power generated from the ASE was almost independent of the input signal power until the pump power reached 800 mW at which the on-off Raman gain was about 24 dB. Hence, the OSNR (P_{sig}/P_{ASE}) increased by an equal amount of signal power increment (Fig. 7). Since the attenuation of the SMF was 17.1 dB, including both input and output connectors, it could be made

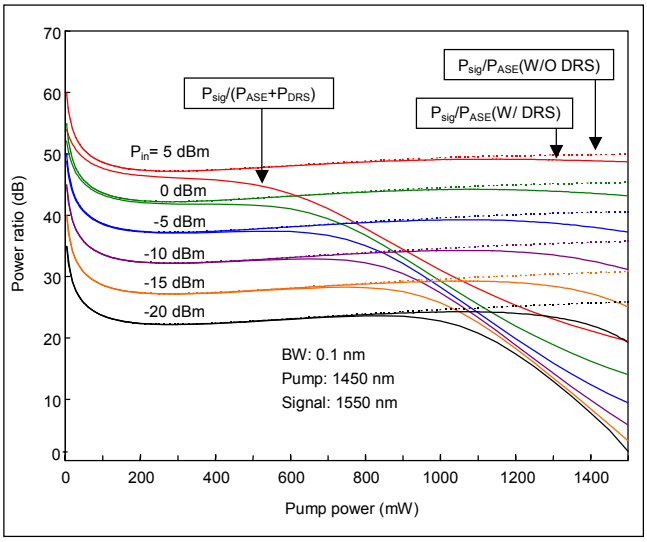

Fig. 7. OSNR versus pump power with and without DRS noise for various input power levels. Thick solid lines, narrow solid lines, and dotted lines indicate $P_{sig}/(P_{ASE}+P_{DRS})$, P_{sig}/P_{ASE} with DRS, and P_{sig}/P_{ASE} without DRS, respectively.

lossless when the pump power was higher than 600 mW (Fig. 6). The equivalent noise figure at a pump power of 600 mW was about –2 dB.

When the DRS of both the signal and the ASE was taken into account, the noise characteristics changed. In this case, the optical noise power included both the ASE power (P_{ASE}) and the DRS power of the signal (P_{DRS}), where the ASE power consisted of the ASE power generated by the Raman process and the DRS of the ASE. In Fig. 7, the OSNR, which is the power ratio of the output signal to optical noise ($P_{sig}/(P_{ASE}+P_{DRS})$), decreased again as the pump power increased and there were local maxima for input powers lower than 0 dBm. For higher input power, the OSNR degraded monotonically. P_{DRS} was proportional to the signal input power at low pump powers and the amount was not comparable to P_{ASE} unless the input power was larger than 0 dBm. However, P_{DRS} grew faster than the signal gain as the pump power increased and it eventually exceeded P_{ASE}. Hence, the OSNR limitation appeared at a much lower pump power range than when only the DRS of the ASE was considered (Fig. 7), which was the case examined by Hansen et al [15]. When the crosstalk from the DRS of the signal was calculated as a function of on-off Raman gain for various input powers, the crosstalk was uniquely determined by gain, regardless of the input power (Fig. 8). Since the power penalty due to DRS of a signal is given by (9) [16],

$$\delta_I = -10\log_{10}\left(1-\frac{1}{2}\frac{P_{DRS}}{P_{sig}}NQ^2\right), \qquad (9)$$

where N and Q are the number of spans and system Q, respectively, the crosstalk that gives a power penalty of 0.1 dB after13 span (> 1000 km) at a bit error ratio of 10^{-12} (Q=7.03) was calculated to be 41.5 dB corresponding to an on-off gain of

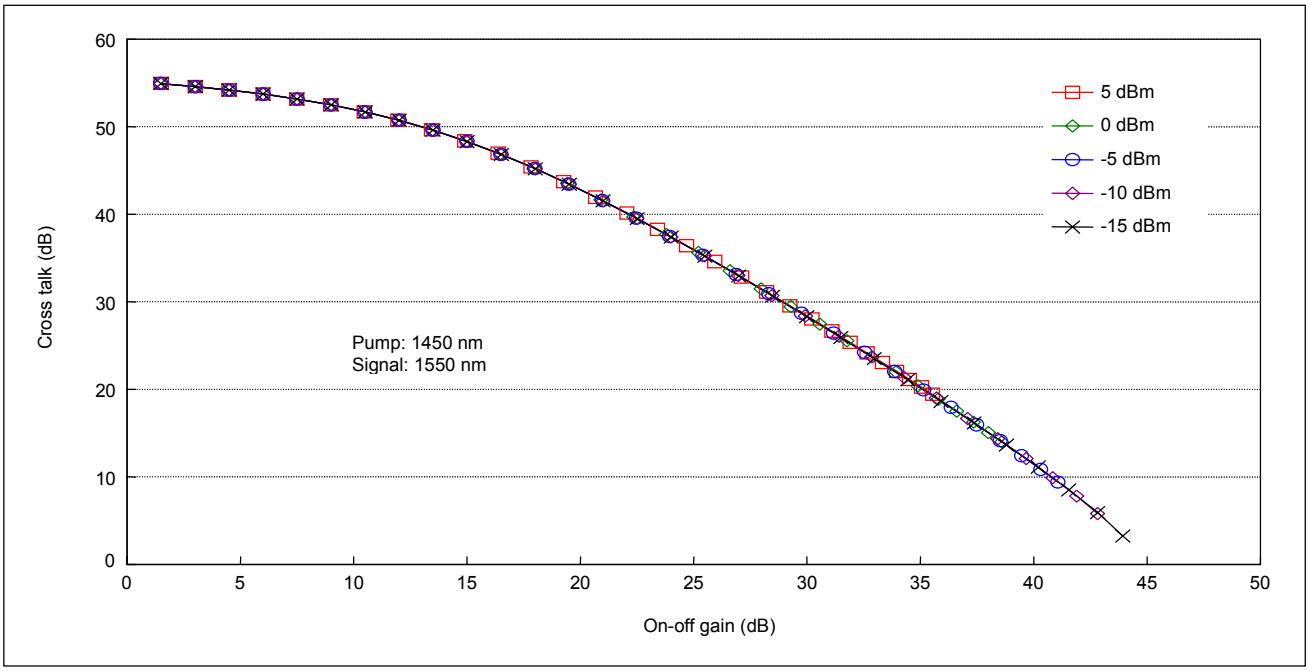

Fig. 8. DRS of signal induced crosstalk versus on-off Raman gain.

about 21 dB. Therefore, the DRS noise can be ignored when the Raman gain is below 21 dB, which corresponds to a pump power of about 700 mW from Fig. 6.

VI. MULTIPLE CHANNEL AMPLIFICATION

For multiple channel amplification, our aim was to accommodate 160 channels in both C-band (1530.0–1562.0 nm) and L-band (1571.0–1605.0 nm) with channel spacing of 50 GHz, where 80 channels were equally allocated to each band. Since the wavelength shift of the peak Raman gain from the pump wavelength is about 100 nm in the 1500 nm region, 1445 nm and 1485 nm can be the simplest combination of the Raman pump wavelengths. In a DRA, however, the pump with the shorter wavelength transfers its energy not only to WDM signal channels but also to the pump with the longer wavelength as it passes through a long length of fiber. Consequently, a two or three times larger pump power is normally required for the shorter wavelength pump than the longer wavelength pump in order to uniformly amplify both the C- and L-bands. Therefore, it is necessary to allocate two pump wavelengths for C-band amplification when pump LDs with finite pump power are to be used. When a commercial PWC capable of multiplexing 4 pump wavelengths with equal spacing is considered, roughly five possibilities can be listed in selecting two pump wavelengths for C-band and one for L-band, where the shortest pump wavelength is kept less than or equal to 1430 nm in order to minimize OSNR degradation due to the gain tilt arising from the SRS effect between signal channels. Cases A, B, and C have wavelength spacing of 25 nm while cases D and E have 20 nm (Table 1). In order to determine the optimum pump wavelength combination, the pump power of the shortest wavelength was fixed at a maximum available value. To our knowledge, currently the maximum power of the fiber coupled output from a single wavelength stabilized LD with a fiber Bragg grating (FBG) is 230 mW. The maximum insertion losses of the PBC, PWC, and PSWC (Fig. 1) are 0.4, 0.8, and 0.4 dB, respectively, so that the overall insertion loss before launching into the SMF should be 2 dB including the splice losses. Therefore, the output power of the two polarization multiplexed LDs becomes 290 mW at the SMF input. In the numerical simulation, input signal power per channel was assumed to be 1.0 dBm, so that the total 160 channel input would be 23 dBm.

Table 1. Five different Raman pump wavelength combinations.

	Ch 1 (nm)	Ch 2 (nm)	Ch 3 (nm)	Ch 4 (nm)
A	1420	1445	(1470)	1495
B	1425	1450	(1475)	1500
C	1430	1455	(1480)	1505
D	1425	1445	(1465)	1485
E	1430	1450	(1470)	1490

At first, the pump powers of the first and second wavelength were maximized. Then, the pump power of the third wavelength was increased until the L-band output power became equal to the C-band. If the average gain per band was below 10 dB, they were considered to be optimum pump power values. If it exceeded 10 dB, the pump power of the second wavelength was lowered until it got close to 10 dB and the output power of each band was balanced using the third wavelength. The resultant optimum pump powers and the corresponding gains and output powers are summarized in Table 2. In cases A, B, and C, the average gains did not reach 10 dB and the output power excursions were larger than those in cases D and E (Fig. 9, 10). In cases D and E, 10 dB gains were achievable with the pump powers at a second wavelength of above 250 mW and 240 mW for D and E, respectively. Case D had lower output power excursion than case E, but case E had the advantage when the extension of the gain bandwidth to the longer wavelength side was considered in L-band. Between these two fac

Table 2. Optimum pump powers for the 2nd and 3rd pump wavelengths for each pump wavelength combination at maximum pump power of the 1st pump wavelength, and the corresponding gain, output power, and output power excursion.

	$P_{pump,2nd}$ (mW)	$P_{pump,3rd}$ (mW)	$G_{on\text{-}off,avg}$ (C) (dB)	$G_{on\text{-}off,avg}$ (L) (dB)	P_{out} (C) (dBm)	P_{out} (L) (dBm)	ΔP_{out} (C) (dB)	ΔP_{out} (L) (dB)
A	290	108	9.39	9.57	12.2	12.2	2.63	2.45
B	290	122	9.72	9.93	12.6	12.6	2.25	2.77
C	290	122	9.72	9.87	12.5	12.5	2.53	2.43
D	250	160	10.17	10.33	13.0	13.0	1.71	1.90
E	240	160	10.18	10.33	13.0	13.0	2.28	2.00

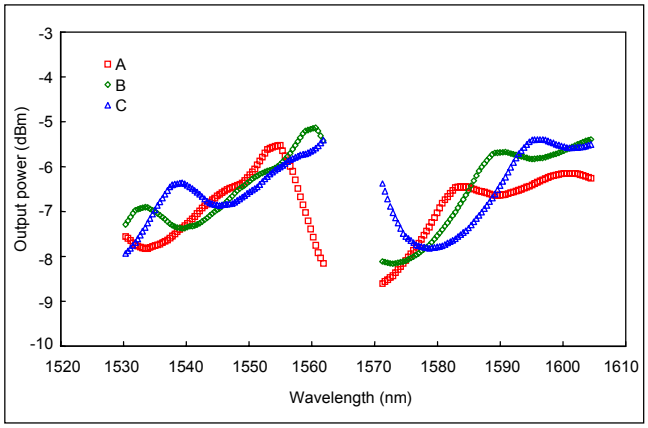

Fig. 9. Output power spectrum of 160 channels for various pump wavelength combinations. See Table 1 for meaning of A, B, and C.

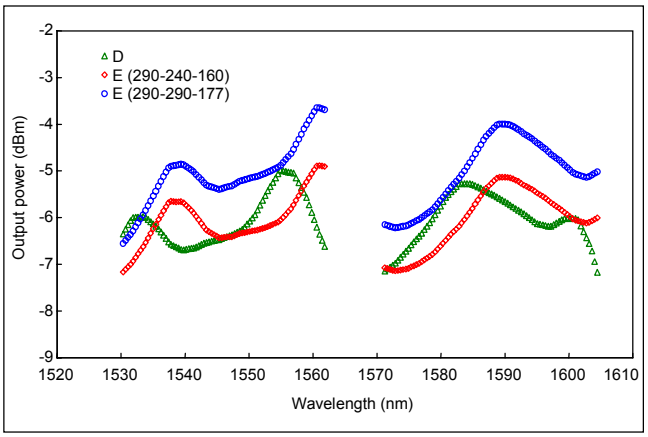

Fig. 10. Output power spectrum of 160 channels for various pump wavelength combinations. See Table 1 for meaning of D and E. The numbers in parentheses correspond to pump powers for successive wavelengths in mW.

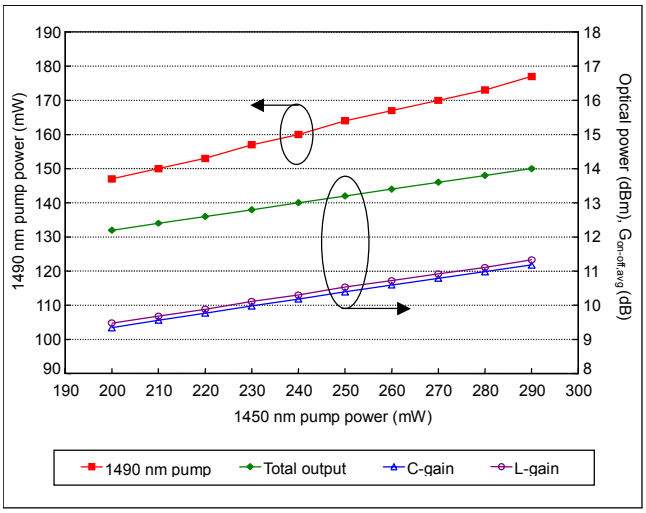

Fig. 11. Required pump power of 1490 nm pump versus pump power of 1450 nm when the pump power of 1430 nm was fixed at maximum. The second Y-axis correspond to total output power in dBm and average on-off Raman gain for C- and L-band in dB scale.

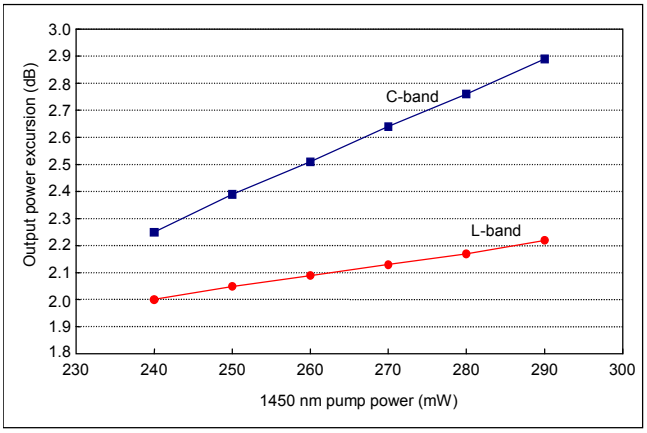

Fig. 12. Output power excursion versus pump power of 1450 nm. 1430 nm and 1490 nm pump conditions were the same as in Fig. 10.

tors, the output power excursion or gain flatness of the Raman amplifier itself is of less importance in the hybrid amplifier design because the quantity is small compared to that of the EDFA, and it can be easily compensated for by a gain flattening filter (GFF) inserted between the GB1 and GB2 of the EDFA. Consequently, case E was chosen for the optimum pump wavelength combination for the DRA.

For case E, we examined the DRA characteristics as we increased the pump power of 1450 nm and maximized that of 1430 nm while we correspondingly adjusted that of 1490 nm so that both C- and L-band output power would be equal. As the pump power of 1450 nm increased, the adjusted pump power of 1490 nm increased linearly and so did the output power in the log scale (Fig. 11). The output power excursion in the log scale was also linearly proportional to the 1450 nm pump power (Fig. 12). As we expected from the previous single channel analysis, the DRS in this case did not cause any effect, because the gain was less than 12 dB at best. The OSNR increment due to DRS was no greater than 0.04 dB with a 0.1 nm filter bandwidth. The NF ranged from –2.2 to +2.2 dB depending on the wavelengths as plotted in Fig. 13. Owing to the 1490 nm pump and SRS effect, the NF profile has a negative slope in the wavelength domain [17]. Figure 14 shows the power evolution of the 3 backward pumps and 8 sampled channels for each band, where C-band channels experienced higher attenuation than L-band channels before amplification. As mentioned earlier in this section, the energy transfer from the shorter wavelength pumps to the longer wavelength pump

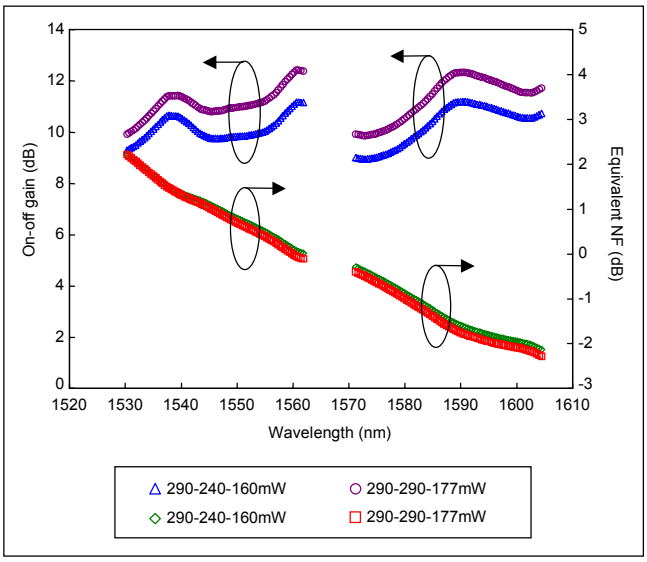

Fig. 13. On-off Raman gain and NF spectrum for two pump power combinations.

Table 3. Simulation parameters for EDFA.

Parameter	Value	Tolerance
Cut-off wavelength	895 nm	±5 %
Loss at 1558.5 nm	1.95 dB/m	±5 %
Core radius	1.47 μm	±5 %
Refractive index difference (Δn)	0.0184	±5 %
Numerical aperture	0.233	±5 %
Peak absorption (near 1.53 μm)	5.53 dB/m	±5 %
Peak absorption (near 980 nm)	4.05 dB/m	±5 %
MFD (Petermann 2) 1.55 μm	5.75 μm	±5 %
Background loss 1.2 μm	4.08 dB/km	±5 %
Estimated background loss 1.55 μm	1.58 dB/km	±5 %
Fiber outside diameter	125 μm	±2 μm
Estimated erbium concentration	8.1×10^{24} m^{-3}	

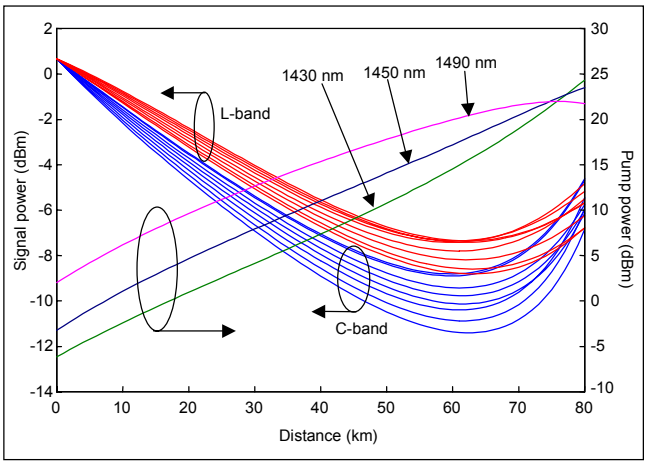

Fig. 14. Evolution of signal and pump power. For signal evolution, 8 channels were sampled for each band with 5 nm spacing including the first and the last channels.

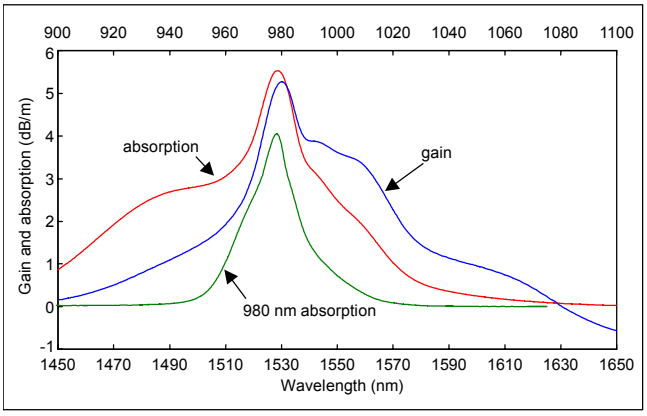

Fig. 15. Measured spectrum of absorption and gain per unit length of the used erbium-doped fiber.

occurred because of the SRS effect (Fig. 14), which explains why only 23 percent of the total launched pump power was required at the pump wavelength of 1490 nm in order to balance the output power of C- and L-bands.

VII. ERBIUM-DOPED FIBER AMPLIFIER

The calculated output from the DRA was then sent to the GB1 of the following EDFAs. In order to characterize the performance of the hybrid amplifier theoretically, the C-band EDFA was simulated exemplarily. Table 3 shows the parameters of the EDF used for simulation. In the EDFA simulation, we used the equation shown in Ref. [18], [19] with measured absorption and emission data (Fig. 15) supplied by the manufacturer. The modal intensity profile was assumed to be Gaussian. Since the input power of GB1 was higher than 5 dBm, including the insertion loss of the PCM and C/L-band splitter, both forward and backward pumping with full available power at 980 nm in GB1 was assumed, that is 180 mW. To maximize the output power, the EDF of GB2 was assumed to be pumped by the forward and backward 1480 nm pump with an output power of 200 mW. The PSWC for combining the pump and signal is assumed to be a WDM/Tap Coupler/Isolator hybrid type for forward pumping and a WDM/Isolator hybrid type for backward pumping. The insertion loss of the PSWC was set to 1.4, 0.8, 0.8, and 0.8 dB for 980 nm forward, 980 nm backward,

1480 nm forward, and 1480 nm backward, respectively, with signal ports, and 0.6 dB for all pumps with pump ports, in accordance with the data sheet of commercial products. The splice loss between the 980 nm WDM coupler and the EDF was about 0.2 dB for both 980 nm and 1550 nm. For the 1480 nm WDM coupler, it was about 0.8 dB for both the pump and signal wavelengths. Therefore, the overall insertion loss for the signal band was assumed to be 2.0, 1.9, 2.6, 2.5 dB for GB1 input, GB1 output, GB2 input, and GB2 output, respectively, including the input and output fiber connectors, additional tap couplers for backward pumping, and some margin for estimation errors. The overall insertion loss for the pump band was assumed to be 0.8, 0.8, 1.4, and 1.4 dB, respectively.

Between GB1 and GB2, the inter-stage containing the VOA, GFF, and DCM was considered with a maximum insertion loss of 16.5 dB assumed. A simulation program calculated the filter profile of the inter-stage to obtain flattened output for all channels. After the total output power and the gain profile of GB2 were calculated with a flat input profile, the required input profile that produced the flat output profile with the same total output power negligibly changed the gain profile. The gain difference was less than 0.01 dB. Therefore, the desired input profile was obtained from the flat output profile producing the same output power divided by the gain profile calculated using the flat input profile. The filter profile of the inter-stage could then be calculated by comparing the output profile of GB1 and the input profile of GB2. Once the inter-stage filter profile was obtained, the gain, NF, and the output power of GB2 were calculated again using the changed input profile to confirm the correct result.

When the average gain and NF of GB1 over 80 channels was calculated as a function of the EDF length, the maximum output power of 20.66, 20.74, and 20.86 dBm could be obtained at a length of 18, 16–18, 14–16 m, for the input power of 0, 5, and 10 dBm, respectively. After these optimum lengths were reached, output power decreased because the unpumped region began to appear. There was a tendency for the optimum length to be shorter for higher input power. The higher input power caused faster decay of the pump, so the unpumped region began to appear at a shorter EDF length. The NF was an increasing function of the EDF length. If the EDF length was increased with a fixed pump power, the average population inversion decreased and the spontaneous emission factor increased to give a higher NF. Figure 16 shows the average gain and NF as a function of input power when the length of the EDF was 10, 12, and 14 m, respectively. The minimum NF of 5.1 dB was located at an input power of between –6 and –7 dBm for an EDF length of 10m. It corresponded to an internal NF, of the EDF itself, of 3.1 dB, which is close to the limit of a discrete amplifier. The input power for the local minimum NF moved to a higher value, about –4 dBm for 16 m, as the EDF length increased. After a 5 dBm input, the NF increased steeply. It is possible to obtain an output power of more than 20 dBm as long as the input power is greater than 0 dBm with an EDF length longer than 10 m.

Unlike GB1, the output power of GB2 had no local maximum until the EDF length reached 22 m. This was because the 1480 nm pump had a slower absorption rate than the 980 nm

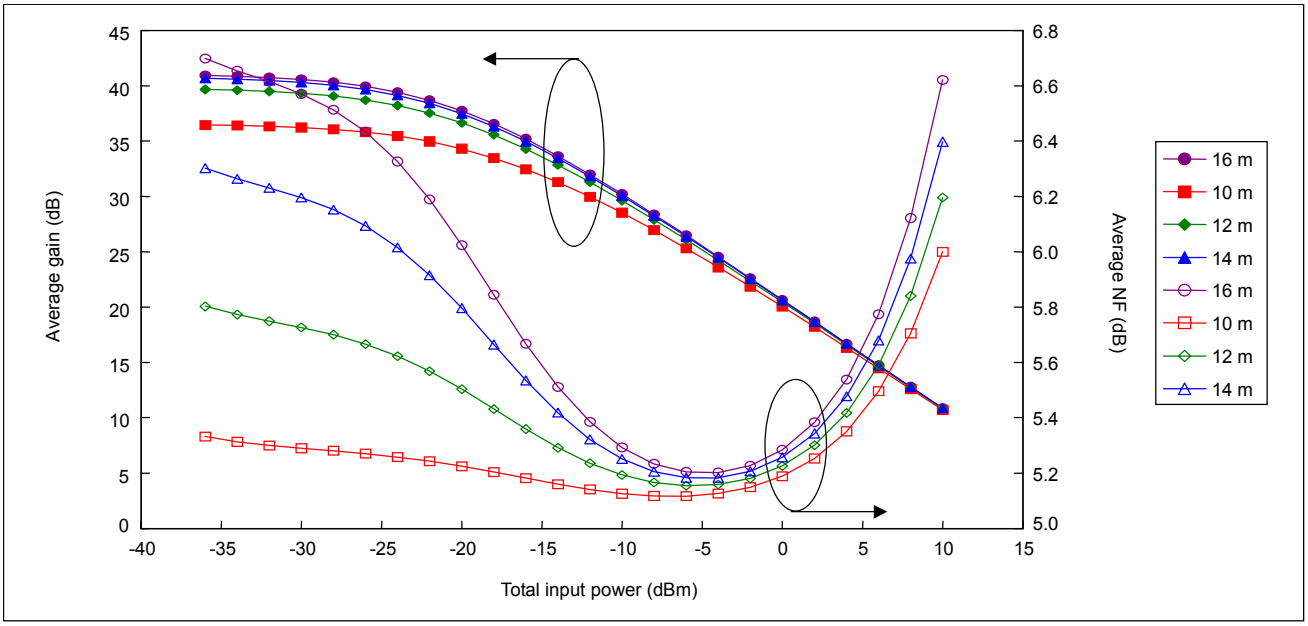

Fig. 16. Average gain and NF versus input power for various EDF lengths in GB1.

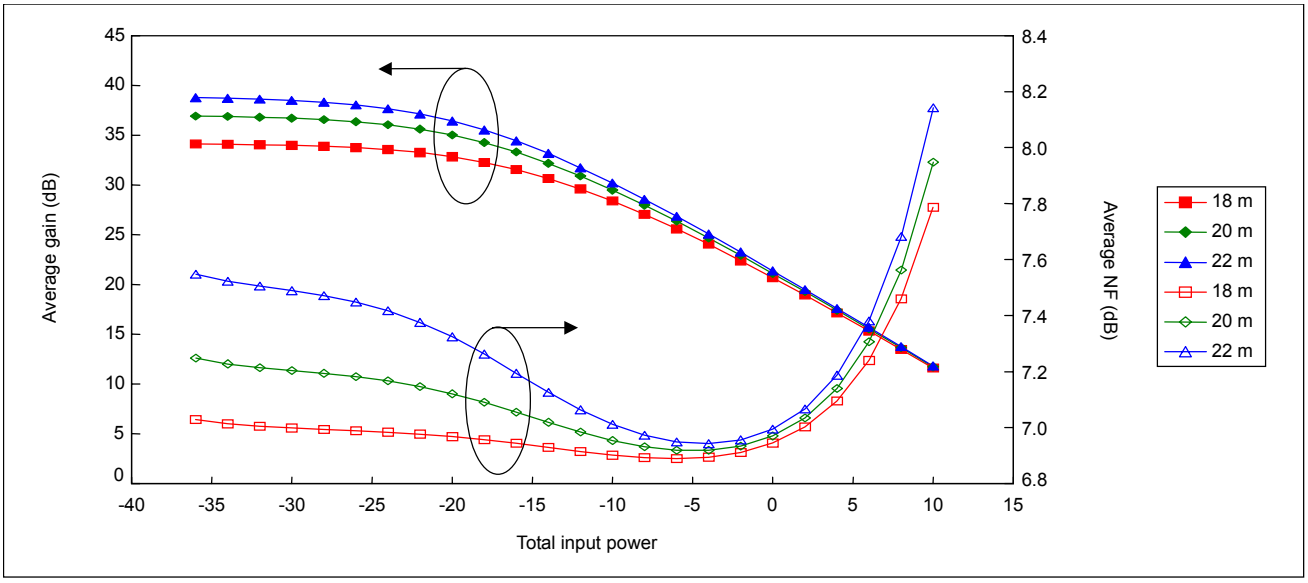

Fig. 17. Average gain and NF versus input power for various EDF lengths in GB2.

pump. The EDF length necessary to achieve more than 21 dBm output power was 20 m for 0 dBm input and 18 m for 5 dBm input. Since the maximum output power from GB1 was about 20 dBm or more, the input power to GB2 was at least about 3.5 dBm if the inter-stage loss of 16.5 dB was considered. Therefore, the length of EDF for GB2 should be longer than 18 m. Figure 17 shows the average gain and NF of GB2 as a function of input power. The average NF is basically larger than that of GB1 because the average inversion is low.

The total NF profiles of the EDFA (GB1+GB2) was then calculated for several EDF length combinations including the about 1 dB insertion loss of the C/L-band WDM splitter and combiner when the fiber transmission loss was assumed to be 22 dB so that the input power might be –2 dBm. The increment of the EDF length from 10 to 14m in GB1 uniformly reduced the NF, but the effect was negligible after 14 m. However, the EDF length change in GB2 produced rotation in the NF profile with the pivot point at about 1546 nm (Fig. 18), and it rotated counterclockwise as the length increased. The flattest NF profile can be achieved with a length of 17 m. However, the output power did not reach 20 dBm for 17 m, so that the optimum length design was determined to be 14 m for GB1 and 18 m for GB2.

VIII. PERFORMANCE OF THE HYBRID AMPLIFIER

Assuming that the input power per channel, gain, and NF of the optical boosting amplifier (OBA) were –20 dBm, 21 dB, and 6 dB, respectively, we estimated the OSNR trace of the cascaded amplifier without Raman pumping as shown in Fig. 19.

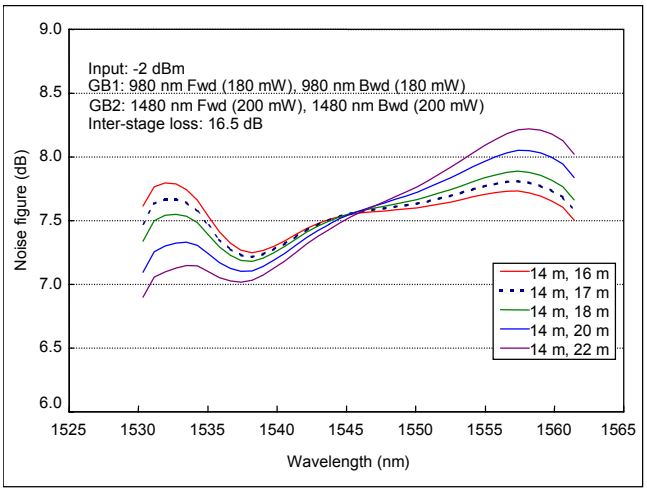

Fig. 18. NF spectrum of EDFA for various EDF length in GB2 when the EDF length of GB1 was 14 m and the Raman pump was off.

The wavelength dependence of fiber loss and the SRS effect were not taken into account in the calculation. Because the NF profile had the minimum and maximum values depending on the wavelength in Fig. 18, the OSNR trace also had the minimum and maximum values although the gain flatness was less than 0.003 dB. After 10 spans, the OSNR became 21.2–22.2 dB.

For the Raman pumping, the input power of the EDFA was set at 5 dBm using the PCM function and considering the design margin and the additional minimum insertion loss of the PSWC and PCM, which was assumed to be about 2 dB. Then, the fiber transmission loss could be effectively reduced to 15

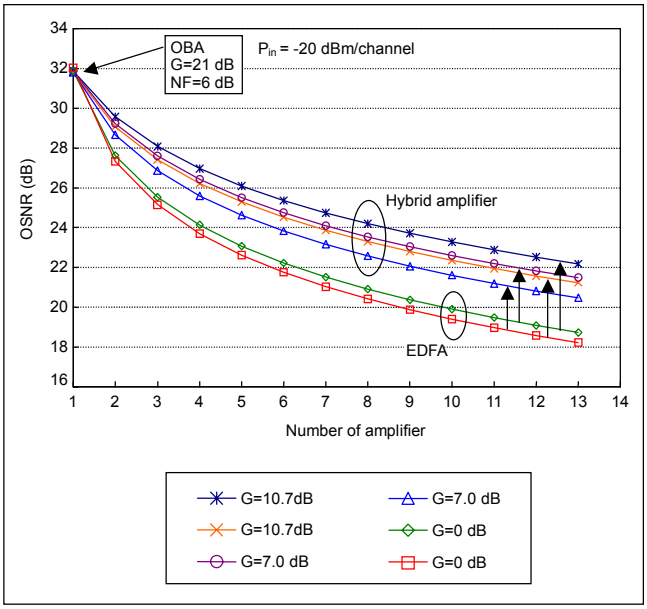

Fig. 19. OSNR traces for optical link with span loss of 22 dB. The upper four traces correspond to minimum and maximum OSNR depending on wavelength for hybrid amplifier, while the lower traces for EDFA.

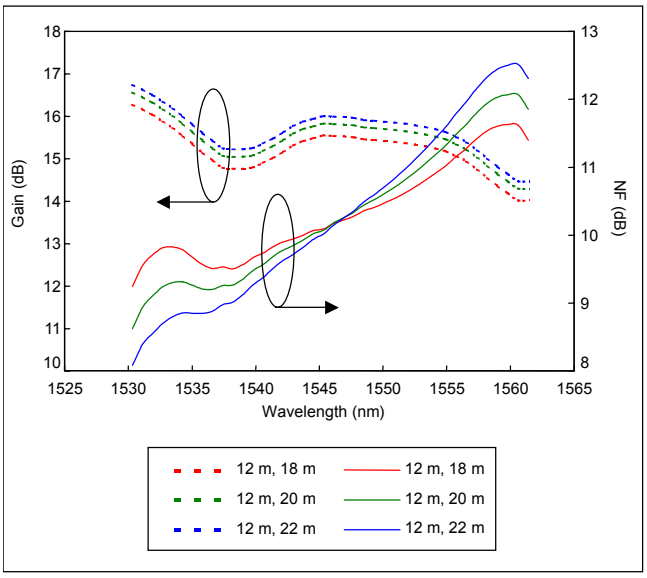

Fig. 20. Gain and NF spectrum of EDFA for various EDF length in GB2 when the EDF length of GB1 was 12 m and the Raman pump was on.

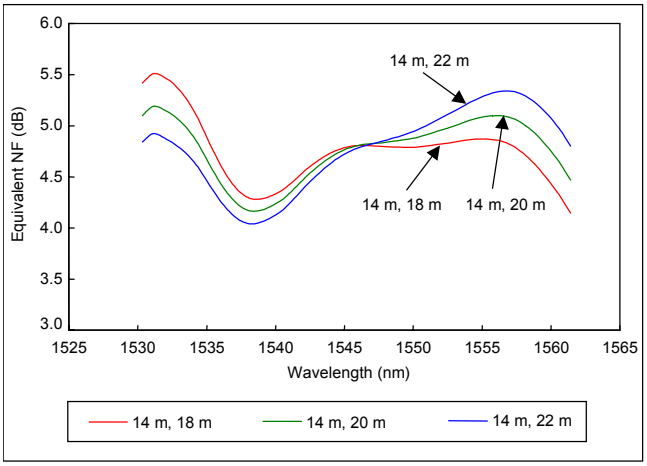

Fig. 21. Total equivalent NF of hybrid amplifiers for various EDF length in GB2 with EDF length in GB1 of 14 m.

dB. Since the input profile to the EDFA was not flat due to the Raman gain profile, the gain of the EDFA had inverted profiles of Raman gain to produce a flat output power profile (Fig. 20). With this high input power, the NF of the EDFA ranged from about 8 dB to about 13 dB depending on the EDF length. The effect of a change in EDF length was similar to the case of –2 dBm input.

In order to find the optimum length of EDF in the hybrid amplifier design, the equivalent amplifier concept was used. Using the same measured attenuation coefficient, the fiber length was increased so that the average fiber attenuation over the wavelength range would be equal to 22 dB. The output from the fiber, which was –2 dBm, was conceptually thought to be the input of the hybrid amplifier. The hybrid amplifier was treated as a discrete amplifier with an on-off gain and equivalent NF. Both the wavelength dependent fiber attenuation and SRS effect were included in the on-off Raman gain to compare the result with the case without the Raman amplifier. Then the NF of the hybrid amplifier was between 4.1 and 5.3 dB (Fig. 21). Since the NF of the Raman amplifier had a negative slope (Fig. 13), the total NF became flat with an EDF length of 20 m for GB2 because the slope was well compensated for by the positive slope of the NF of the EDFA shown in Fig. 20. The optimum EDF length for GB1 seemed to be 14 m but the effect was less than 0.2 dB compared with 10 m in terms of NF. The optimum EDF length for GB2 was determined to be 20 m from Fig. 21. Figure 22 shows the calculated filter profile of the inter-stage, in which the background loss for DCM and VOA was subtracted. It seems that the case of 10 m for GB1 and 20 m for GB2 is more desirable than the other two in fabricating the gain flattening filter.

In order to evaluate the validity of the simulation result, the GFF profile estimated by simulation was compared with the experimentally measured GFF profile (Fig. 23). The GFF profile was for the EDFA only, where the EDF length was 18 m for GB1 and 20 m for GB2. The main difference came from the fact that the simulated GFF profile included the wavelength dependent loss of the DCM whereas the measured GFF profile excluded the DCM. When the DCM loss profile was

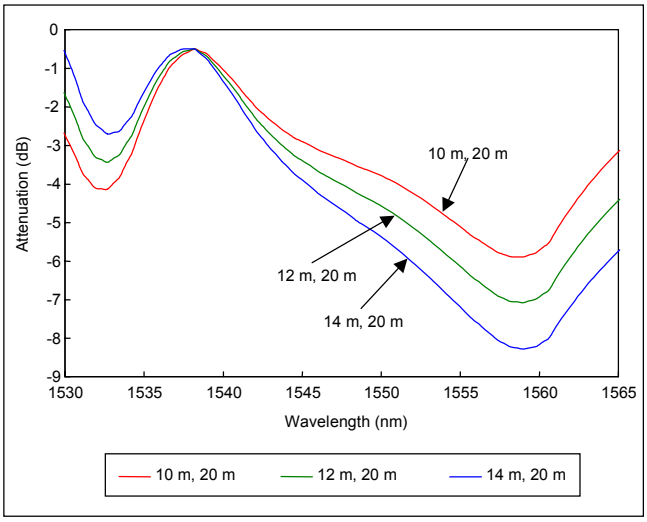

Fig. 22. Estimated inter-stage filter profiles to produce flat output of EDFA.

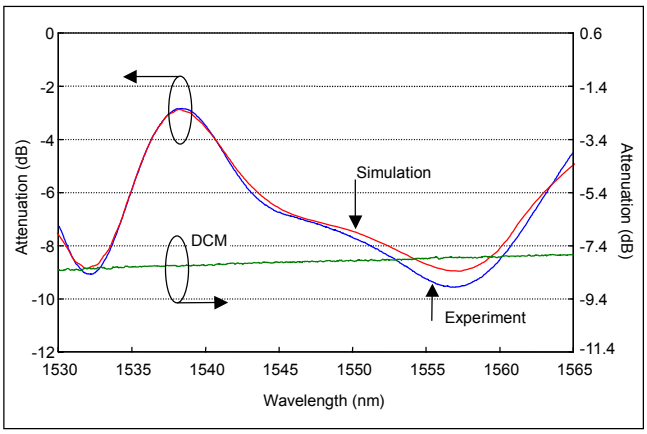

Fig. 23. Comparison of GFF profiles between simulation and experiment for EDFA with EDF length for GB1 and GB2 of 18 m and 20 m, respectively.

separately measured and drawn together (Fig. 23), the discrepancy was compensated for.

The OSNR trace of the cascaded hybrid amplifier was estimated as shown in Fig. 19. In comparison with the EDFA without a DRA, the average OSNR was improved by 2.5 dB after 10 spans when the Raman gain was 7.0 dB, including the insertion loss of the PSWC and PCM. This was improved by 3.2 dB over the EDFA without a DRA when the Raman gain was raised to 10.7 dB by increasing the 1450 nm pump fully and re-adjusting the 1490 nm pump correspondingly, at which time the PCM was removed and the GFF profile was reshaped while the EDF length remained unchanged. The insertion loss of the PSWC was assumed to be 1.0 dB. The equivalent NF in this case was reduced to 3.4–4.5 dB. Figure 24 shows how the

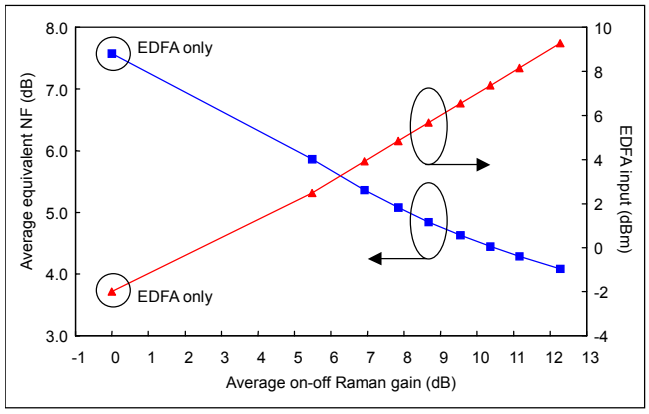

Fig. 24. Average equivalent NF versus average on-off Raman gain and the corresponding input power to EDFA.

average equivalent NF changed as the Raman gain increased. It is clear that the increasing Raman gain was advantageous in reducing the overall NF, although the NF of the EDFA increased as the input power grew (Fig. 16). This fact can be explained by (10), which is derived from the NF equation of cascaded optical amplifiers [18],

$$\Delta NF = \Delta NF_{DRA} + \frac{NF_{EDFA} - A}{G_{DRA} A}\left(\frac{\Delta NF_{EDFA}}{NF_{EDFA} - A} - \frac{\Delta G_{DRA}}{G_{DRA}}\right), \tag{10}$$

where A is the attenuation between the DRA and EDFA, which was 1.0 dB. Since NF_{DRA} is negative and $(NF_{EDFA} - A)$ is positive, (10) is negative if the parenthesis is negative, which applies when the increasing rate of the NF of the EDFA is smaller than the DRA gain increasing rate. In Fig. 25, the average NF of the EDFA increased by about 0.6 dB for a 1 dB increment of the average DRA on-off gain.

VIV. CONCLUSIONS

Our study examined the characteristics of the DRA and EDFA in order to achieve the optimum design for hybrid optical amplifiers. Our results showed that the DRS noise induced power penalty became negligible after 13 spans of 80 km SMF as long as the on-off Raman gain of the DRA was less than 21 dB. We determined that the three optimum pump wavelengths for an amplification bandwidth of 32 nm for C-band and 34 nm for L-band were 1430, 1450, and 1490 nm. Using commercially available fiber optic components with highest pump LDs, the on-off gain of the DRA comprising those three pump wavelengths was more than 11 dB. The total equivalent NF of the hybrid amplifier decreased as the gain of the DRA increased as long as the rate of increase of the NF for the EDFA was smaller

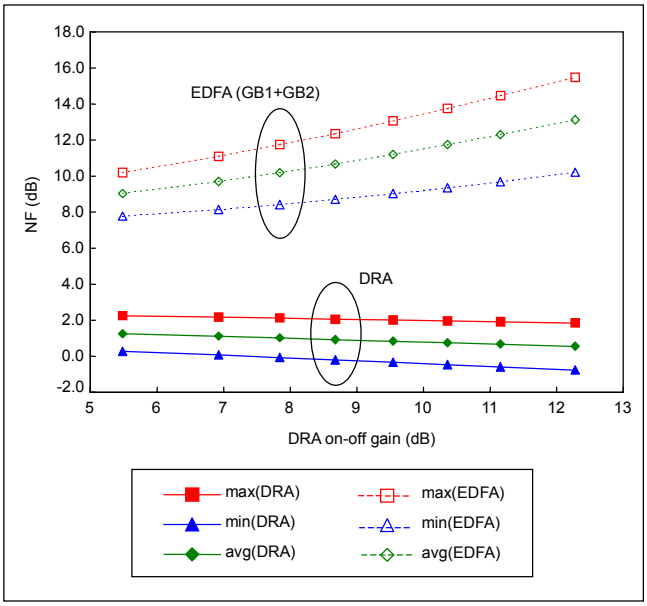

Fig. 25. Maximum, minimum, and average NF for DRA and EDFA, respectively, as a function of on-off Raman gain.

than the rate of increase of the gain for the DRA. For the fiber optic transmission link with a 22 dB span loss, our hybrid amplifier improved the OSNR after 10 spans by 3.2 dB over the EDFA without a DRA.

REFERENCES

[1] T.N. Nielson, "Raman Amplifiers in WDM Systems," *12th LEOS Annual Meeting*, vol. 2, 1999, pp. 471-472.

[2] T. Tsuzaki, M. Kakui, M. Hirano, M. Onishi, Y. Nakai, and M. Nishimura, "Broadband Discrete Fiber Raman Amplifier with High Differential Gain Operating over 1.65 μm-Band," *Optical Fiber Comm. Conf.* (Anaheim, CA, 2001), MA3.

[3] S. Kawai, H. Masuda, K. Suzuki, and K. Aida, "Wide-Bandwidth and Long-Distance WDM Transmission Using Highly Gain-Flattened Hybrid Amplifier," *IEEE Photon. Technol. Lett.*, vol. 11, no. 7, 1999, pp. 886-888.

[4] W.Y. Oh, S.S. Lee, H. Lee, and W. Seo, "16-Channel C-Band Hybrid Fiber Amplifier Comprising an EDFA and a Single Diode Laser Pumped Dispersion Compensating Raman Amplifier," *European Conf. On Comm.* (Munich, Germany, 2000), 4.4.5.

[5] H. Suzuki, J. Kani, H. Masuda, N. Takachio, K. Iwatsuki, Y. Tada, and M. Sumida, "1-Tb/s (100×10Gb/s) Super-Dense WDM Transmission with 25-GHz Channel Spacing in the Zero-Dispersion Region Employing Distributed Raman Amplification Technology," *IEEE Photon. Technol. Lett.*, vol. 12, no. 7, 2000, pp. 903-905.

[6] Y. Zhu, W.S. Lee, C. Scahill, C. Fludger, D. Watley, M. Jones, J. Homan, B. Shaw, and A. Hadjifotiou, "1.28Tbit/s (32×40Gbit/s) Transmission over 1000 km NDSF Employing Distributed Raman Amplification and Active Gain Flattening," *Electron. Lett.*, vol. 37, no. 1, 2001, pp. 43-45.

[7] B. Zhu, P.B. Hansen, L. Leng, S. Stulz, T.N. Nielsen, C. Doerr, A.J. Stentz, D.S. Vengsarkar, Z.J. Chen, D.W. Peckham, and L. Gruner-Nielsen, "800 Gbit/s (80×10.66Gbit/s) Transmission over 3200 km of Non-Zero Dispersion Shifted Fibre with 100 km Amplified Spans Employing Distributed Raman Amplification," *Electron. Lett.*, vol. 36, no. 22, 2000, pp. 1860-1861.

[8] T.N. Nielsen, A.J. Stentz, K. Rottwitt, D.S. Vengsarkar, Z.J. Chen, P.B. Hansen, J.H. Park, K.S. Feder, S. Cabot, S. Stulz, D.W. Peckham, L. Hsu, C.K. Kan, A.F. Judy, S.Y. Park, L.E. Nelson, and L. Gruner-Nielson, "3.28-Tb/s Transmission over 3×100 km Nonzero-Dispersion Fiber Using Dual C- and L-Band Distributed Raman Amplification," *IEEE Photon. Technol. Lett.*, vol. 12, no. 8, 2000, pp. 1079-1081.

[9] J.S. Wey, D.L. Butler, M.F. Leeuwen, L.G. Joneckis, and J. Goldhar, "Crosstalk Bandwidth in Backward Pumped Fiber Raman Amplifiers," *IEEE Photon. Technol. Lett.*, vol. 11, no. 11, 1999, pp. 1417-1419.

[10] G.P. Agrawal, *Nonlinear Fiber Optics, 3rd ed.*, Academic Press, San Diego, 2001, pp. 298-303.

[11] B. Min, W.J. Lee, and N. Park, "Efficient Formulation of Raman Amplifier Propagation Equations with Average Power Analysis," *IEEE Photon. Technol. Lett.*, vol. 12, no. 11, 2000, pp. 1486- 1488.

[12] R.H. Stolen, "Nonlinear Properties of Optical Fibers," in *Optical Fiber Telecommunications*, S.E. Miller and A.G. Chynoweth, ed. Academic Press, San Diego, 1979, p. 130.

[13] B.H. Choi, M.J. Chu, H.H. Park, and J.H. Lee, "Performances of Erbium-Doped Fiber Amplifier Using 1530 nm-Band Pump for Long Wavelength Multichannel Amplification," *ETRI J.*, vol. 23, no. 1, 2001, pp. 1-8.

[14] H. Kidorf, K. Rottwitt, M. Nissov, M. Ma, and E. Rabarijaona, "Pump Interactions in a 100-nm Bandwidth Raman Amplifier," *IEEE Photon. Technol. Lett.*, vol. 11, no. 5, 1999, pp. 530-532.

[15] P.B. Hansen, L. Eskildsen, A.J. Stentz, T.A. Strasser, J. Judkins, J.J. DeMarco, R. Pedrazzani, and D.J. DiGiovanni, "Rayleigh Scattering Limitations in Distributed Raman Pre-Amplifiers," *IEEE Photon. Technol. Lett.*, vol. 10, no. 1, 1998, pp. 159-161.

[16] M. Nissov, K. Rottwitt, H.D. Kidorf, and M.X. Ma, "Rayleigh Crosstalk in Long Cascades of Distributed Unsaturated Raman Amplifiers," *Electron. Lett.*, vol. 35, no. 12, 1999, pp. 997-998.

[17] C.R.S. Fludger, V. Handerek, and R.J. Mears, "Fundamental Noise Limits in Broadband Raman Amplifiers," *Optical Fiber Comm. Conf.* (Anaheim, CA, 2001), MA5.

[18] E. Desurvire, *Erbium-Doped Fiber Amplifiers: Principles and Applications*, John Wiley & Sons, New York, 1994, Ch. 1, Ch. 2.

[19] T.G. Hodgkinson, "Improved Average Power Analysis Technique for Erbium-Doped Fiber Amplifiers," *IEEE Photon. Technol. Lett.*, vol. 4, no. 11, 1992, pp. 1273-1275.

Seung Kwan Kim received his BS degree in physics from Seoul National University, Seoul, Korea, in 1991. He received MS and PhD degrees in physics from KAIST, Daejeon, Korea, in 1993 and 1997, respectively. From 1997 to 1998, he visited the Optoelectronics Division at the University of Strathclyde in Glasgow, Scotland, where he worked on tunable fiber lasers. In 1999, he joined ETRI, Daejeon, Korea, where he has been involved in research and development on multiwavelength fiber lasers, high power EDFAs, and fiber Raman amplifiers for high capacity WDM transmission system. Dr. Kim is a member of OSK and OSA.

Sun Hyok Chang received his BS degree in physics from Korea Advanced Institute of Science and Technology (KAIST) in 1994. He received MS and PhD degrees in physics from KAIST in 1996 and 2000, respectively. He joined Electronics and Telecommunications Research Institute in 2000 and has been engaged in research on WDM fiber optic telecommunication systems. He is currently interested in fiber Raman amplifiers and nonlinear effects in the transmission fibers. Dr. Chang is a member of the Optical Society of Korea (OSK).

Jin Soo Han received his BE degree in electronic engineering from Yonsei University, Seoul, Korea, in 1998. He received his ME degree from Korea Advanced Institute of Science and Technology, Daejeon, Korea, in 2000, and he joined Electronics and Telecomm- unications Research Institute, Korea. His resear- ch interests are optical communication system, WDM transmission technology, and optical network.

Moo Jung Chu received his BS degree in physics from Yonsei University, Seoul, Korea, in 1980. He received MS and PhD degrees from Korea Advanced Institute of Science and Technology, Daejeon, Korea, in 1982 and 1985, respectively. In 1985, he joined Electronics and Telecommunications Research Institute (ETRI), Korea. He is a Principal Member of Optical Communications Department, ETRI. He has been engaged in research of optical devices, optical amplifiers, WDM optical transmission technology. Dr. Chu is a member of KITE, KICS, OSK, and Korea Physical Society.